Plasmonics (2023) 18:1477–1488
https://doi.org/10.1007/s11468-023-01874-1

RESEARCH

# Numerical Study of Titanium Dioxide and MXene Nanomaterial-Based Surface Plasmon Resonance Biosensor for Virus SARS-CoV-2 Detection

Swati Srivastava[1] · Sachin Singh[1] · Adarsh Chandra Mishra[1] · Pooja Lohia[2] · D. K. Dwivedi[1]

Received: 30 March 2023 / Accepted: 28 April 2023 / Published online: 11 May 2023


## Abstract

A novel surface plasmon resonance-based biosensor for SARS-CoV-2 virus is proposed in this article. The biosensor is a Kretschmann configuration-based structure that consists of $CaF_2$ prism as base, at which silver (Ag), $TiO_2$, and MXene nanolayers are used to enhance the performance. Theoretically, the performance parameters have been investigated by means of Fresnel equations and transfer matrix method (TMM). The $TiO_2$ nanolayer not only prevents oxidation of Ag layer but also enhances the evanescent field in its vicinity. The sensor provides an ultrahigh angular sensitivity of 346°/RIU for the detection of SARS-CoV-2 virus. Some other performance parameters, including FWHM (full width at half maxima), detection accuracy (DA), limit of detection (LOD), and quality factor (QF) have also been calculated for proposed SPR biosensor with their optimized values 2.907°, 0.3439 $deg^{-1}$, $1.445 \times 10^{-5}$, and 118.99 $RIU^{-1}$, respectively. The obtained results designate that the proposed surface plasmon resonance (SPR) based biosensor has notably enhanced angular sensitivity as compared to previous results reported in the literatures till date. This work may facilitate a significant biological sample sensing device for fast and accurate diagnosis at early stage of SARS-CoV-2 virus.

**Keywords** Coronavirus disease · Nanomaterials · Thiol-tethered DNA · Ligand · Angular sensitivity

## Introduction

The emergence of novel viruses has always led to pandemics and economic and social disruption, affecting health and keeping millions of lives at risk [1, 2]. The outbreak of the fatal coronavirus (COVID-19) caused by severe acute respiratory syndrome coronavirus 2 (SARS-CoV-2) was a paramount worldwide health issue. A clump of pneumonia of unknown origin was identified in December 2019 [3], which was eventually declared a deadly pandemic by World Health Organization (WHO). Normally, the concerned virus, i.e., the SARS-CoV-2 virus, is a single-stranded RNA virus and contains four significant proteins, which are the spike glycoprotein (S), nucleocapsid proteins (N), membrane protein (M), and envelope protein (E) that are being used for detection [4]. The spike glycoprotein (S) has two subunits, S1 and S2, among which S1 protein tends to bind with the receptor on the surface of target cells, i.e., ACE2 (angiotensin-converting enzyme 2) [5, 6]. ACE2 protein is present in lung (type I also type II alveolar epithelial cells), heart, kidney, nasal and oral mucosa, and brain, therefore easily providing a path for the S1 virus protein to invade the cells [4]. Eventually, causing massive damage to the heart, kidneys, and brain. The neutralization of these S1 virus proteins is the main concern of research and for the invention of effective vaccines for SARS-CoV-2 virus. The crucial detection of SARS-CoV-2 spike protein demands a quick, appropriate, but also significantly sensitive way to monitor. There are various conventional techniques for the early-stage diagnosis of the concerned virus, such as the chest computed tomography (CT) scan [7], RNA detection using reverse transcription-polymerase chain reaction (RT-PCR) technique [8, 9], reverse transcription loop-mediated isothermal amplification (RT-LAMP) [10], and enzyme-linked immunosorbent assay (ELISA) [7]. Clashing with the requirements, RT-PCR assay is quite time-consuming; it may take 4 h to execute a single test and still has considerable probability of false-negative results also CT scans require trained radiologists and cannot be afforded by rural hospitals; likewise, every other technique has some distinct drawbacks.

✉ D. K. Dwivedi
todkdwivedi@gmail.com

1 Photonics and Photovoltaic Research Lab, Department of Physics and Material Science, Madan Mohan Malaviya University of Technology, Gorakhpur 273010, India

2 Department of Electronics and Communication Engineering, Madan Mohan Malaviya University of Technology, Gorakhpur 273010, India

An emerging branch of biosensor known as the surface plasmon resonance (SPR)-based biosensor is being recommended because of its quick, accurate, real-time mapping, label-free, and highly sensitive response [11]. Due to its above properties, it is used in various fields of medical diagnostics, biotechnology [12], and as detection technique for novel viruses, influenza H1N1 [13], EV71 virus [14], and formalin detection [15]. In accordance with the above advantages, it is also involved in the identification of the respiratory syndrome coronavirus. The electrons at the interface of metal-dielectrics get stimulated with the help of p-polarized light, and their collective oscillation gives rise to phenomenon of SPR. After resonance, a sharp dip of reflected light intensity is perceived, known as the resonance curve. Among all the configurations, the Kretschmann configuration is being considered because of its simplicity and ease of experiment. The attenuated total reflection (ATR) method, being the working principle for reflectance curve, is prominently controlled by the angular interrogation approach. An SPR biosensor consisting of $MoSe_2$ and graphene (C) was designed for the specific detection of coronavirus spike (S) protein by Moznuzzaman et al. [16]. Sachin et al. reported a graphene-coated multilayer SPR-based biosensor for the expeditious detection of fatal coronavirus [17]. Silicon nitride employed SPR biosensor was proposed by Kumar et al. for the detection of same [18]. Gold nanospike film was used to develop a sensing device for the detection of the presence and concentration of antibodies particular to the SARS-CoV-2 spike protein [19].

Two-dimensional nanomaterials (2D-nanomaterials) have allured plenty of interest in recent years as a consequence of their excellent electrooptic characteristics [20, 21] in SPR biosensors. They offer enhanced chemical and physical functionality owing to their ultrathin structure, high surface-to-volume ratio, and surface changes [22]. MXene is quite beneficial than other 2D nanomaterials because of its two primary properties, metallic conductivity and hydrophilicity [23]. Therefore, $Ti_3C_2T_X$ is considered a favorable material for increasing the sensitivity of a SPR biosensor. Qiong Wu et al. reported MXene utilized SPR sensor for the ultrasensitive carcinoembryonic antigen detection [24]. MXene-employed SPR sensor for detecting the COVID virus was proposed by Chen et al. [25] MXene-coated PCF for detection of cancer cells was also proposed by Kumar et al. [26] Transition metal dichalcogenides (TMDCs) with configuration ($MX_2$) show unique optoelectronic properties than their individual components. They behave like a 2D semiconductor with direct bandgap lying in the visible and near IR range. Because of this behavior, $MX_2$ has acquired interest in SPR biosensors for biological/chemical detection [27]. $TiO_2$ has a high light trapping capability because of which more SPs are generated that ultimately increase the resonance angle, leading to an enhancement in the sensitivity of the biosensor [16]. $TiO_2$ employed surface plasmon resonance-based biosensors that have been reported for detection of cancer cells [28]. Karki et al. reported a $TiO_2$-$SiO_2$ layers-based biosensor for formalin detection [15].

The present paper proposes a configuration in which $TiO_2$ and $Ti_3C_2T_X$ are employed for the detection of the concerned virus, i.e., SARS-CoV-2 virus. Configuration of structure I is $CaF_2$ prism/Ag/$TiO_2$/SM, that of structure-II is $CaF_2$ prism/Ag/$Ti_3C_2T_X$/SM, and that of structure-III is $CaF_2$ prism/Ag/$TiO_2Ti_3C_2T_X$/SM. The layers of 2D nanomaterials and metal are deposited in accord with the Kretschmann configuration at the base of employed coupling prism. With the help of TMM method, the three structures are theoretically investigated. The reflectance curve for varying angles of incidence is plotted for all three structures. Moreover, the performance parameters, namely angular sensitivity (S), detection accuracy (DA), fixed width at half maxima (FWHM), quality factor (QF), and limit of detection (LOD) are also calculated and summarized in Table 3. A comparative study for various thicknesses of $TiO_2$ layer in the final configuration is also conducted. This study may facilitate an accurate and fast sensing device for early-stage diagnosis of concerned coronavirus. The three proposed structures, along with their assembling, are provided in Table 1.

## Proposed Design Contribution and Mathematical Modeling

### The Proposed Sensor Configuration

A simplified illustration of the proposed SPR biosensor with $CaF_2$/Ag/$TiO_2$/MXene/sensing medium configuration for the detection of SARS-CoV-2 virus is conveyed in Fig. 1. A p-polarized light from the 633 nm wavelength source is directed in one side of the $CaF_2$ prism, and simultaneously, at the other side of the coupling prism, reflected light is detected. Electrons of light beam entirely reflected at boundary produces an evanescent wave that interacts with the plasma wave when metal has appropriate thickness. The reflected light can be detected with the help of detector and computer system. Moreover, as depicted in Fig. 1, the structure is based on Kretschmann configuration.

**Table 1** Proposed structures and layer arrangement of proposed SPR based biosensor

| Respective structures | Assembling of films |
|---|---|
| Structure-I | $CaF_2$ prism/Ag/$TiO_2$/SM |
| Structure-II | $CaF_2$ prism/Ag/$Ti_3C_2T_X$/SM |
| Structure-III | $CaF_2$ prism/Ag/$TiO_2$/$Ti_3C_2T_X$/SM |

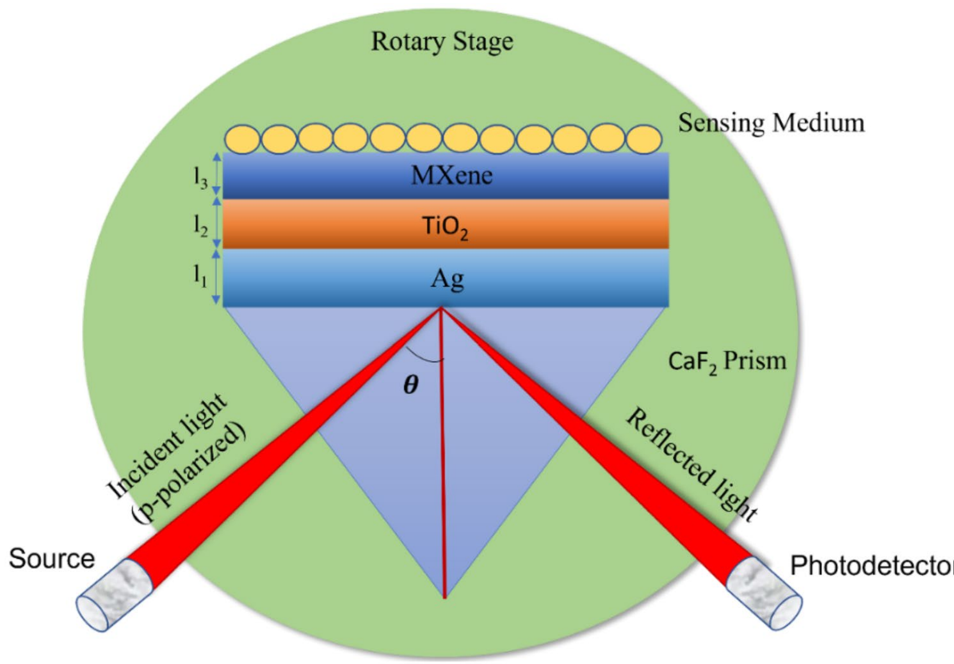


**Fig. 1** Schematic structure of the proposed five-layer SPR based biosensor

***Layer 1: A Light Coupling Prism ($CaF_2$)*** In the current article, calcium fluoride glass prism, i.e., $CaF_2$ prism, is utilized as a coupling substrate. In context of better rejection of angular error, the low RI value of the $CaF_2$ prism is beneficial during the setup [29]. On top of that, the low refractive index substrate aids in providing maximum angular sensitivity and great shift in reflectance curve as compared to another prism for the proposed biosensor, as shown in Fig. 1. The RI of $CaF_2$ is computed using the Sellmeier equation [30].

$$\left(n_{\mathrm{CaF-2}}\right)^2 = [1.33973 + \frac{0.69913 \times \lambda^2}{\lambda^2 - (0.09374)^2} + \frac{0.11994 * \times\lambda^2}{\lambda^2 - (21.18)^2} + \frac{4.35181 \times \lambda^2}{\lambda^2 - (38.46)^2}] \tag{1}$$

Here, "$\lambda$" is the wavelength of the incident light in nanometers.

***Layer 2: SPR-Active Metal Silver (Ag)*** The second layer is the SPR-active metal silver (Ag) layer, which can be deposited upon the prism by thermal vapor deposition technique. In context of providing a narrow resonance curve, Ag is better than Au (gold) [31]. But the oxidation of Ag layer reduces the lifetime of SPR biosensor. The complex RI value of Ag layer can be conveyed using the well-known Drude–Lorentz model [32],

$$n_{\mathrm{Ag}}^2 = \varepsilon_{\mathrm{Ag}} = \left[1 - \frac{\lambda_c \times \lambda^2}{\lambda_p^2\left(\lambda_c + i\lambda\right)}\right] \tag{2}$$

Here, $\lambda_c$ is the collision wavelength and $\lambda_p$ is the plasma wavelength of metallic layer. The numerical value of $\lambda_p$ and $\lambda_c$ for Ag are $1.4591 \times 10^{-7}$ and $1.7614 \times 10^{-5}$ m, respectively. $\lambda$ is the wavelength of the incident monochromatic light, i.e., $\lambda = 633$ nm.

***Layer 3: Titanium Dioxide Layer ($TiO_2$)*** To overcome the major issue of oxidation of Ag layer and the subsequent issue of reduction of lifetime, a layer of titanium dioxide ($TiO_2$) is deposited over the Ag layer. It is a metal oxide and has good conductivity, which does shift the functional wavelength to the near IR region. There are some added beneficial properties such as greater electrochemical stability, non-toxicity, less carrier concentration (nearly 1020–1022/cm$^2$), and resistance to corrosion mechanism that makes it suitable for the SPR biosensor [33].

The dispersion formula calculates the RI value of $TiO_2$ at wavelength 633 nm and is given as

$$n(\lambda) = \sqrt{\varepsilon_{\mathrm{TiO_2}}(\lambda)} = \left[5.913 + \frac{2.441 \times 10^7}{\lambda^2 - 0.843 \times 10^7}\right]^{\frac{1}{2}} \tag{3}$$

Here, λ is the wavelength of the incident light in $A^0$ units.

***Layer 4: A Monolayer of MXene ($Ti_3C_2T_X$)*** The layer of $TiO_2$ is further covered by a monolayer of MXene ($Ti_3C_2T_X$). The heterojunction formed by $TiO_2$ and $Ti_3C_2T_X$ monolayer will also avert the possible oxidation of Ag. The optimum thickness of $Ti_3C_2T_X$ is 0.993 nm, and the complex RI value of MXene layer is calculated by the following relation given as [34]:

$$n_{\mathrm{MXene}} = 2.380 + 1.33 \times \mathrm{i} \tag{4}$$

At a wavelength of 633 nm.

The ligand layer for the sensing medium used is a thiol-tethered ssDNA, as it has shown notable properties as a receptor for the concerned respiratory syndrome coronavirus [35]. Ultimately, phosphate–buffered saline (PBS) solution is used as the sensing medium. The RI value of the PBS solution can be expressed from the following relation given by:

$$\Delta n_{SM} = 1.334 + \Delta n_{SM} \quad (5)$$

Here, $\Delta n_{SM}$ is the change in RI value because of analyte-ligand interaction in the sensing surface when the concerned virus is added to the sensing medium. It is already mentioned that the SARS-CoV-2 glycoprotein can dissolve in a running buffer containing 120 mM NaCl solution and 10 nM HEPES solution [35]. A linear relation is obtained between the RI values of HEPES and PBS when different concentrations of HEPES were added to 120 mM of NaCl and given as [36]

$$y_{PBS} = 1.334 + 0.00004 \times x_{HEPES} \quad (6)$$

here, $x$ is the RI of HEPES solution in mM and $y$ is the RI of PBS solution. In the present theoretical study, we have taken 10 mM concentration of HEPES solution, regarding which the RI of bare SM comes out to be 1.334 [37]. The refractive index of each layer at 633 nm wavelength and their optimized thickness are tabulated in Table 2.

## Mathematical Modeling and Method

For determining optical properties like reflectance and transmittance, TMM (transfer matrix method) has been employed. The TMM does not need approximation, allowing it to give highly accurate results. Owing to this advantage, in the present work, the transfer matrix approach for the N-film design and Fresnel equation is utilized to evaluate the reflectance of the projected multilayer design ($CaF_2$ prism/Ag/$TiO_2$/$Ti_3C_2T_X$/sensing medium). The proposed layers are stacked in parallel to one another, and their thickness dk changes perpendicularly along the $z$-axis. The boundary conditions $Z=Z_1=0$ is considered at the first layer interface and $Z=Z_{N-1}$ at the last layer interface. The tangential component of electromagnetic field at the first and last layer boundary has a relation that is given as [33–36]:

$$\begin{bmatrix} E_1 \\ V_1 \end{bmatrix} = Y_{ij} \begin{bmatrix} E_{N-1} \\ V_{N-1} \end{bmatrix} \quad (7)$$

where $V_1$ and $E_1$ address the tangential element of magnetic as well as electric fields at the first layer interface also $V_{N-1}$ and $E_{N-1}$ addresses the same at last layer interface.

$Y_{ij}$ is the element for which the characteristics matrix is as follows:

$$Y_{ij} = \begin{bmatrix} Y_{11} & Y_{12} \\ Y_{21} & Y_{22} \end{bmatrix} = \prod_{k=2}^{N-1} Y_k \quad (8)$$

With,

$$Y_k = \begin{bmatrix} \cos\beta_k & {}^{(-i\sin\beta_k)}/_{q_k} \\ -iq_k\sin\beta_k & \cos\beta_k \end{bmatrix} \quad (9)$$

Here, $Y_{11}$, $Y_{12}$, $Y_{21}$, and $Y_{22}$ represent the transfer matrix elements. $k$ represents any arbitrary number. $q_k$ represents the refractive indices and $\beta_k$ represent the phase thickness of corresponding layers, which are defined as

$$\beta_k = [\frac{2\pi d_k\left(\in_k - n_{CaF-2}^2\sin^2\theta\right)^{1/2}}{\lambda}] \quad (10)$$

$$q_k = [\frac{\left(\in_k - n_{CaF-2}^2\sin^2\theta\right)^{1/2}}{\in_k}] \quad (11)$$

Here, $\in_k$ and $d_k$ is the dielectric constant and thickness of the $k$th layer, respectively. $\lambda$, $\theta$, and $n_{CaF-2}$ are the wavelengths of incident light and incident angle of light and refractive index of the $CaF_2$ prism, respectively. Thus, reflectivity for p-polarized light can be given as

$$R_P = |r|^2 = \left[\frac{(X_{11} + X_{12}q_N)q_1 - (X_{21} + X_{22}q_N)}{(X_{11} + X_{12}q_N)q_1 + (X_{21} + X_{22}q_N)}\right] \quad (12)$$

**Table 2** The RI also the optimized thickness of different layers of proposed biosensor

| Material layer used | Optimized thickness | Refractive index | Dielectric constant | References |
|---|---|---|---|---|
| MXene | 0.993 | 2.38 + 1.33*$i$ | 3.8955 + 6.3308*$i$ | [34] |
| $TiO_2$ | 7 | 2.5837 | 6.6755 | [15] |
| Ag | 45 | 0.056253 + $i$*4.2760 | − 18.2810 + 0.4811*$i$ | [38] |
| $CaF_2$ | - | 1.4329 | - | [32] |

## Experimental Feasibility

The steps of experimental feasibility have been shown in Fig. 2. The proposed SPR sensor consists of multilayer structure based on Kretschmann configuration. These multilayer layers are stacked y physical vapor deposition (PVD), liquid exfoliation (LE), and chemical vapor deposition (CVD) techniques. After that, a sensing medium has also been fixed at which the biomolecules interact with the device.

## Performance Parameters

The performance characterization of any surface plasmon resonance-based biosensor is basically contingent on some factors, which are sensitivity ($S$), full width at half maxima (FWHM), quality factor (QF), detection accuracy (DA), and limit of detection (LOD). To obtain a biosensor with better performance, higher values of the performance parameters are favored, except those of the FWHM and LOD. Also, the QF and the DA (the SNR) obtain a favored high value at the lower value of FWHM [38–40].

***Sensitivity (S)*** The key parameter of SPR biosensor is sensitivity, which is defined as the ratio of the corresponding change in the resonance angle ($\Delta\theta_{res}$) with the variation in the refractive index ($\Delta n$) of the medium. It is mathematically defined as.

$$S = [\frac{\Delta\theta_{res}}{\Delta n}] \tag{13}$$

Usually expressed in the unit (°/RIU).

***Full Width at Half Maxima (FWHM)*** It is certainly a major parameter because most of the other performance parameters are calculated using FWHM. It determines the width of the reflectance curve at half of the curve and is defined as.

$$\text{FWHM} = \frac{1}{2}(\theta_{max} + \theta_{min}) \tag{14}$$

Usually expressed in the unit (deg).

***Detection Accuracy (DA)*** The DA, or signal-to-noise ratio (SNR), of the biosensor can be expressed as the inverse of FWHM.

$$\text{DA} = [\frac{1}{\text{FWHM}}] \tag{15}$$

Usually expressed in the unit (deg$^{-1}$).

***Quality Factor (QF)*** One of the important performance parameters of SPR biosensors is the quality factor, also known as the figure of merit (FOM). It is defined as the ratio of $S$ and FWHM, which is mathematically given as

$$\text{QF} = [\frac{S}{\text{FWHM}}] \tag{16}$$

Usually expressed in the unit (RIU$^{-1}$).

***Limit of Detection (LOD)*** The concentration of biomolecules (analyte) in sensing medium is measured quantitatively by LOD and is mathematically defined as.

$$\text{LOD} = [\frac{\Delta n}{\Delta\theta_{res}} \times 0.005] \tag{17}$$

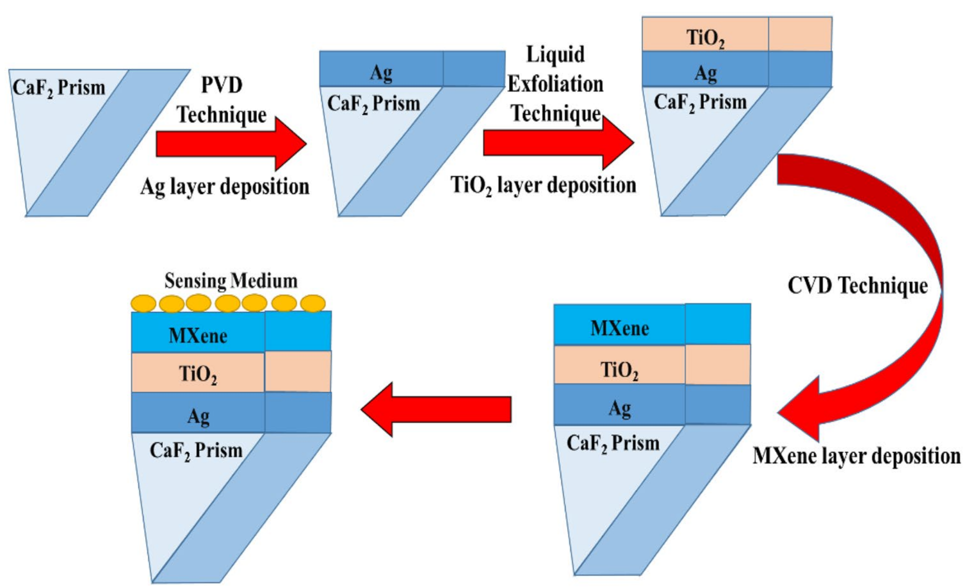


**Fig. 2** Experimental feasibility of proposed SPR sensor

***Electric Field Intensity Enhancement Factor (EFIEF)*** Parameter EFIEF is mathematically defined as the ratio of square of electric field at the last layer interface to electric field at the first layer interface. It is also calculated by the mathematical expression given as

$$\text{EFIEF} = \left| \frac{E(^N/_{N-1})}{E(^1/_2)} \right|^2$$

$$\text{EFIEF} = \frac{\in^1}{\in_N} \left| \frac{V(^N/_{N-1})}{V(^1/_2)} \right|^2 = \frac{\in_1}{\in_N} |t|^2 \quad (18)$$

Here, $t$ being the transmission coefficient and $\in_1$ and $\in_N$ being the dielectric constants.

At the resonance angle, the phase change can be calculated by the given relation

$$\Phi = \arg(r)$$

and

$$r = \tan^{-1}\left(\frac{\text{img } r}{\text{real } r}\right) \quad (19)$$

## Results and Discussion

At the desired resonance condition, a steep dip is perceived in the SPR curve. Any adsorption of any biomolecules on the sensing layer leads to a variation in the RI of the sensing layer, simultaneously leading to the detection of a significant SPR angle shift.

### Selection of $CaF_2$ Prism and Optimization of Ag Layer Thickness

A coupling prism is one of the most important components of a SPR biosensor, as it provides proper synchronization between the surface plasmon wave vector and available tangent component of the wave vector of the incidence light. There are several options for coupling prisms that are being used recently for SPR biosensing. A comparative study for structure-III ($CaF_2$ Prism/Ag/$TiO_2$/$Ti_3C_2T_X$/SM) is done for the selection of most optimal prism between $CaF_2$ (calcium fluoride), BK7 (borosilicate), BAK1 (barium crown), and FK51 (fluorine crown). Considering, $n_1 = 1.350$, $n_2 = 1.355$, with $\Delta n_s = 0.005$, sensitivity is calculated for each prism and conveyed in Fig. 3.

Cadmium fluoride glass prism ($CaF_2$) is considered the coupling prism of the proposed biosensor, as seen in Fig. 3, because $CaF_2$ offers low RI coupling medium and yields maximum angular sensitivity and wide shift in reflectivity as compared to any other prism for the proposed biosensor. An optimal optimization of the used metallic layer is also needed to obtain a near-to-ideal reflectance minimum, i.e., the reflectance minimum must be close to zero. The optimization of Ag layer on considered $CaF_2$ prism is depicted in Fig. 4.

Considering $n_s = 1.334$ different thickness of Ag ($t_{Ag}$) is considered for the reflectance analysis as depicted in Fig. 4. It clearly depicts that minimum reflectance $1.22 \times 10^{-2}$ is obtained at thickness $t_{Ag} = 45$ nm for structure-III $CaF_2$ Prism/Ag/$TiO_2$/$Ti_3C_2T_X$/SM.

The sensing medium here employed is a phosphate-buffered saline (PBS) solution in which the concerned SARS-CoV-2 virus is present. PBS is a water-based salt solution containing disodium hydrogen phosphate, sodium chloride, and in some formulation, potassium chloride and potassium dihydrogen phosphate. The RI of running buffer can be calculated as when certain concentration of 4-(2-hydroxyethyl)-1-piperazine ethane sulfonic acid (HEPES) solution is added into 120 mM sodium chloride (NaCl) solution, a considerable relation between RI of HEPES concentration and running buffer is seen. It is noteworthy that the SARS-CoV-2 glycoprotein easily dissolves in a running buffer containing 120 mM NaCl solution and 10 mM HEPES solution. Succeeding the introduction of the virus in the PBS solution, the RI of the later shifts from 1.334 to 1.355. Four different concentration values are considered varying from 0 mM, 275 mM, 400 mM, and 525 mM mixing in buffer solution. The RI subsequently ranges from 1.334 to 1.355. In context to this incidence, angle versus reflectance curve is analyzed for $n_1 = 1.334$, $n_2 = 1.345$, $n_3 = 1.350$, $n_4 = 1.355$, and an

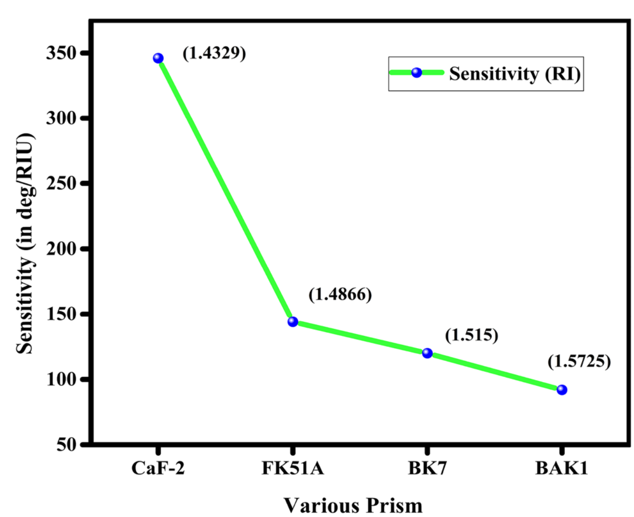


**Fig. 3** Sensitivity versus RI plot for numerous prisms for final structure

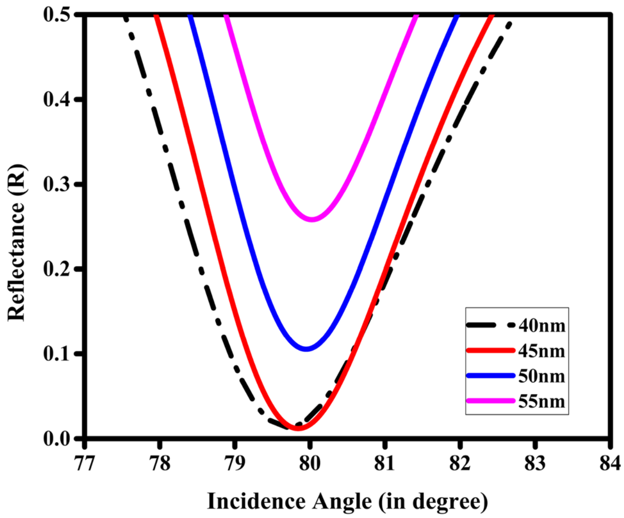


**Fig. 4** Variation of reflectance with incidence angle considering various thicknesses of Ag layer utilized in the proposed SPR biosensor

additional $n_5 = 1.360$. Considering $\Delta n_s = 0.005$, three proposed structures for bio-sensing purpose are indicated with their various performance parameters in Table 3.

In structure-I ($CaF_2$ prism/Ag/$TiO_2$/SM), in bare PBS solution of RI value 1.334, the minimum reflectance is $1.874 \times 10^{-1}$ with a resonance angle of 78.79°. The resonance angle shifts toward a higher resonance angle after the addition of SARS-CoV-2 solution in the sensing layer with minimum reflectance of $1.012 \times 10^{-1}$ and resonance angle of 84.13°. Angular sensitivity is calculated between $n_3 = 1.350$ and $n_4 = 1.355$ with $\Delta n_s = 0.005$. The angular sensitivity obtained is 320°/RIU with FWHM 1.6470° with respect to structure-I, the SPR curve is shown in Fig. 5a. Other parameters such as DA, QF, and LOD are 0.6072 $deg^{-1}$, 194.2926 $RIU^{-1}$, and $1.563 \times 10^{-5}$, respectively.

In structure-II ($CaF_2$ prism/Ag/$Ti_3C_2T_X$/SM), the resonance angle shifts toward a higher resonance angle with resonance angle of 77.47° and minimum reflectance $1.433 \times 10^{-3}$, after the concerned virus solution is added in sensing layer. The performance parameters for this structure are calculated between RI $n_3 = 1.350$ and RI $n_4 = 1.355$ with $\Delta n_s = 0.005$, as shown in Fig. 5b. The required angular sensitivity is 178°/RIU with FWHM of 1.4671°. Other performance parameters such as DA, QF, and LOD are 0.6816 $deg^{-1}$, 121.3277 $RIU^{-1}$, and $2.809 \times 10^{-5}$, respectively.

Proceeding to structure-III ($CaF_2$ prism/Ag/$TiO_2$/$Ti_3C_2T_X$/SM), which is the final structure, to improve the performance parameters to a much greater extent, $Ti_3C_2T_X$ layer is deposited over the $TiO_2$ layer. The resonance angle shifts toward a higher resonance angle with minimum reflectance $1.396 \times 10^{-1}$ and resonance angle of 85.70° after the concerned virus solution is added in sensing layer. The reflectance curve for the respective configuration is shown in Fig. 5c. Angular sensitivity is calculated between $n_3 = 1.350$ and $n_4 = 1.355$ with $\Delta n_s = 0.005$, which is obtained to be 346°/RIU with FWHM 2.9077°. Other performance parameters such as QF, DA, and LOD are 118.99 $RIU^{-1}$, 0.3439 $deg^{-1}$, and $1.445 \times 10^{-5}$, respectively. Notably, it can be perceived that the hybrid structure-III shows much better angular sensitivity and favorable other performance parameters as compared to other structures. The amalgamation of $TiO_2$ and $Ti_3C_2T_X$ is responsible for the angular sensitivity enhancement.

## Comparative Study for Various Thickness of $TiO_2$

The thickness of $TiO_2$ layer plays a major role in improving the sensitivity and other performance of the proposed SPR biosensor. In the final configuration, i.e., in structure-III the thickness of $TiO_2$ has been varied from 1 to 8 nm. Additionally, the performance parameters such as S, QF, FWHM, DA, and LOD were also computed for all configurations, which is briefly summarized in Table 4. It can be easily noted that at 7 nm thickness of $TiO_2$ in final configuration, maximum angular sensitivity 346°/RIU was obtained with FWHM 2.90773° and a minimum LOD of $1.445 \times 10^{-5}$ were obtained and other performance parameters such as DA and QF were 0.3439 $deg^{-1}$ and 118.99 $RIU^{-1}$ were also obtained, respectively. This indicates that the 7 nm thickness of $TiO_2$ is favorable to enhance the angular sensitivity of the biosensor for the detection of the concerned virus as shown in Fig. 6a.

From Table 4, it can be observed that the LOD decreases as the thickness of $TiO_2$ layer is increased to 7 nm. At 7 nm, a minimum LOD $1.445 \times 10^{-5}$ is obtained, which further starts increasing with the increase in the respective thickness. Figure 6b summarizes the variation of FWHM and DA with context to the variation of $TiO_2$ layer thickness.

Furthermore, angular sensitivity with the variation in number of layers of $Ti_3C_2T_X$ is also calculated and

**Table 3** Comparative study of proposed sensors for RI change from 1.350 to 1.355 in sensing medium

| Structures | Sensitivity (deg $RIU^{-1}$) | FWHM (deg) | DA ($deg^{-1}$) | QF ($RIU^{-1}$) | LOD (unitless) |
|---|---|---|---|---|---|
| Structure-I | 320 | 1.6470 | 0.6072 | 194.2926 | $1.563 \times 10^{-5}$ |
| Structure-II | 178 | 1.4671 | 0.6816 | 121.3277 | $2.809 \times 10^{-5}$ |
| Structure-III | 346 | 2.9077 | 0.3439 | 118.9943 | $1.445 \times 10^{-5}$ |

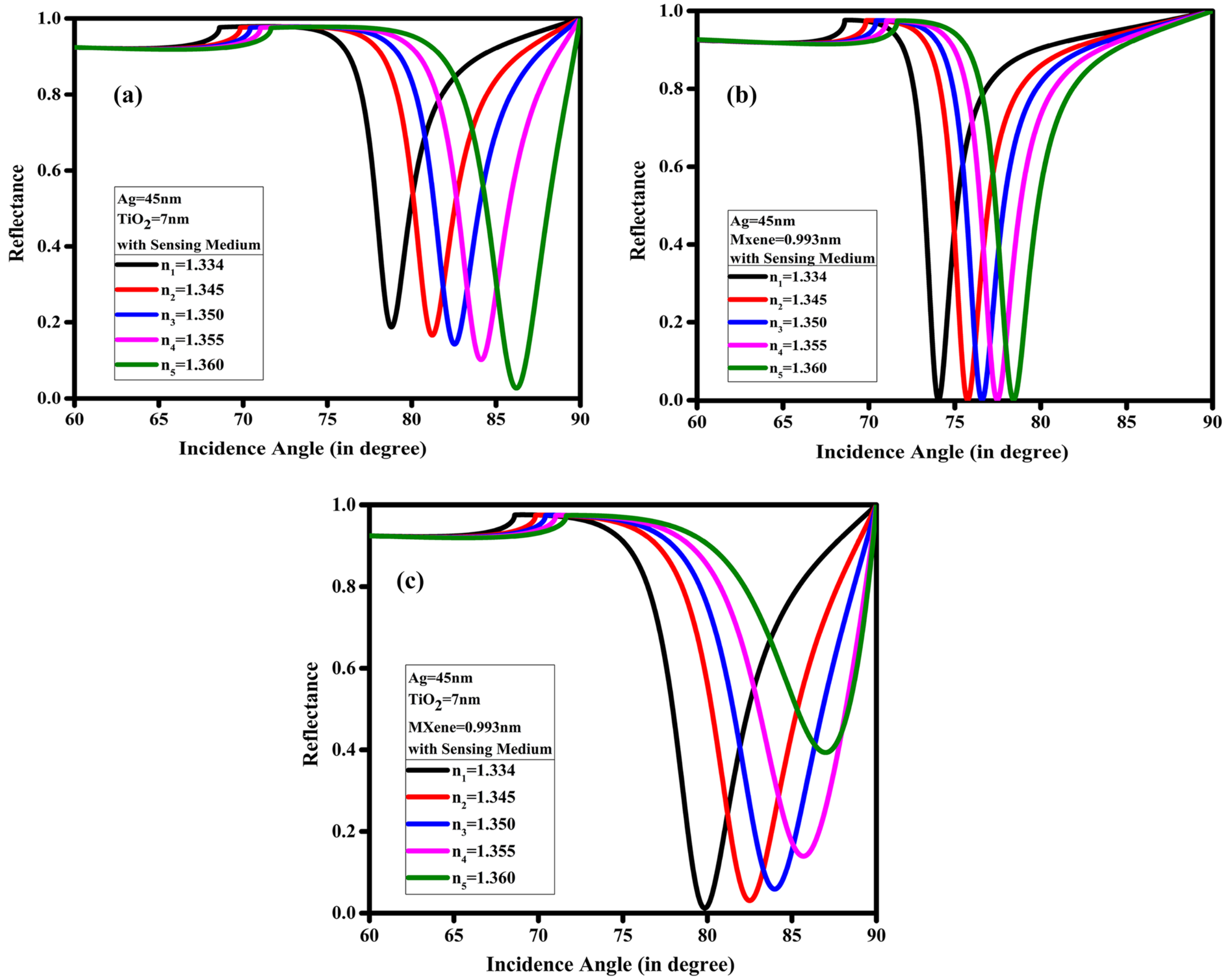


**Fig. 5 a–c** Variation of reflectance with incidence angle for structure-I, II, and III

summarized in Fig. 6c for the final structure ($CaF_2$ prism-Ag-$TiO_2$-$Ti_3C_2T_X$-SM). It can be observed that the angular sensitivity for the proposed biosensor for the concerned virus decreases with the increase in number of layers of MXene. Maximum sensitivity, i.e., 346°/RIU, is observed for monolayer of MXene. In accordance with this, a monolayer of MXene is employed in the proposed biosensor for selective detection.

**Table 4** Comparative study of parameters for various thickness of $TiO_2$ for final structure

| Thickness | Sensitivity (deg $RIU^{-1}$) | FWHM (deg) | Detection accuracy ($deg^{-1}$) | Quality factor ($RIU^{-1}$) | LOD (unitless) |
|---|---|---|---|---|---|
| 1 nm | 186 | 1.64115 | 0.6093 | 113.34 | $2.688\times10^{-5}$ |
| 2 nm | 198 | 1.71604 | 0.5827 | 115.38 | $2.525\times10^{-5}$ |
| 3 nm | 212 | 1.86625 | 0.5358 | 113.59 | $2.358\times10^{-5}$ |
| 4 nm | 232 | 2.0469 | 0.4885 | 113.34 | $2.155\times10^{-5}$ |
| 5 nm | 258 | 2.25867 | 0.4427 | 114.23 | $1.937\times10^{-5}$ |
| 6 nm | 296 | 2.51858 | 0.3970 | 117.53 | $1.689\times10^{-5}$ |
| 7 nm | 346 | 2.90773 | 0.3439 | 118.99 | $1.445\times10^{-5}$ |
| 8 nm | 208 | 4.18486 | 0.2389 | 49.70 | $2.403\times10^{-5}$ |

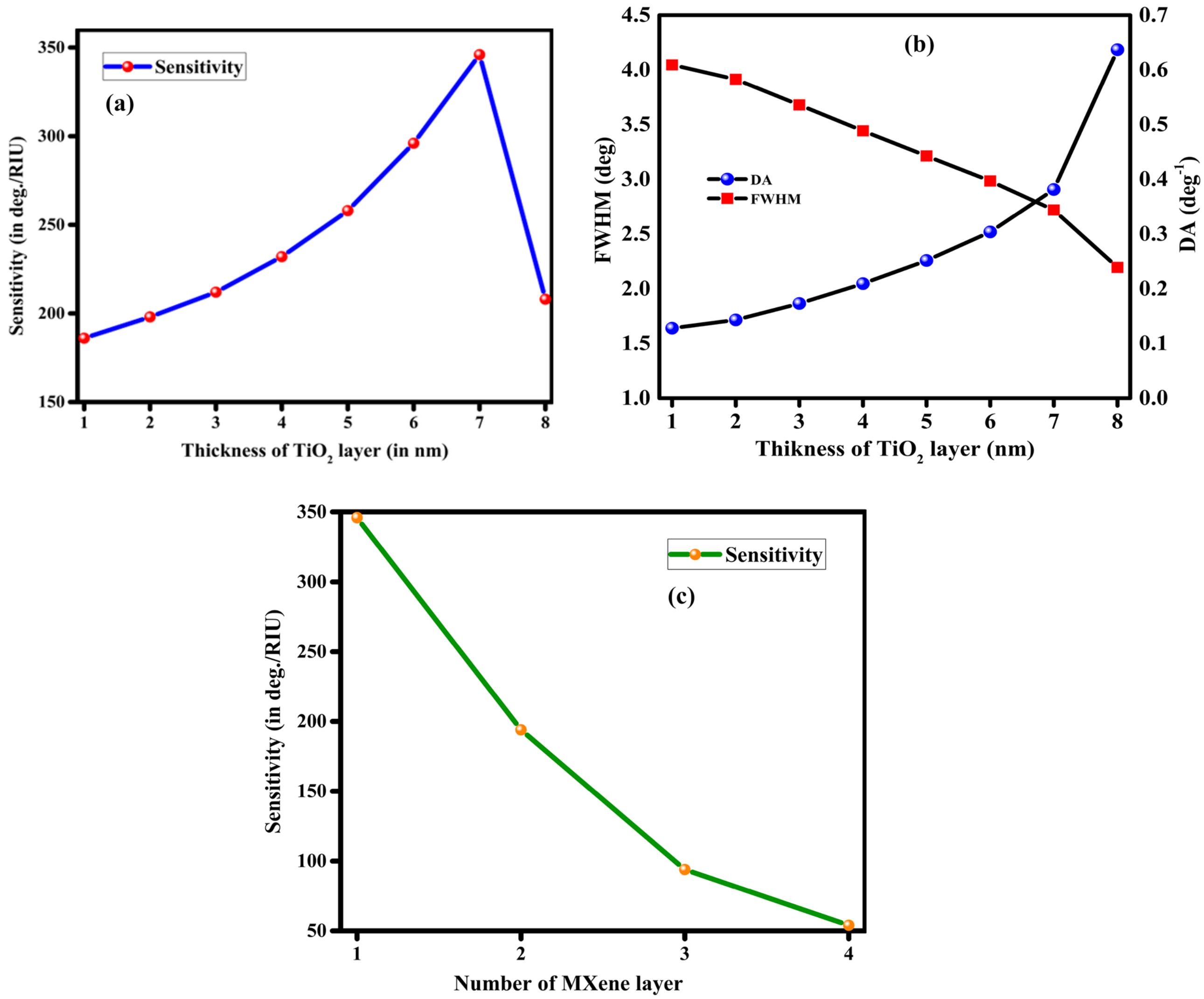


**Fig. 6** **a** Variation in sensitivity in accordance with different thickness of titanium dioxide layer. **b** Thickness of $TiO_2$ layer vs FWHM and DA for final structure. **c** Variation in sensitivity with change in number of layers of MXene

To validate our structure and results, the phase interrogation method has been utilized, which is defined mathematically in (19). The phase change vs the angle of incident for the proposed final structure, i.e., ($CaF_2$ prism/Ag/$TiO_2$/$Ti_3C_2T_X$/SM) has been examined as shown in Fig. 7. It has been observed that at the same corresponding resonance angle, there is an abrupt phase change for the various values of refractive index of sensing medium, from $n_1 = 1.334$ to $n_5 = 1.360$. Figure 6 also shows how the position of phase change is sensitive to any change in refractive index, otherwise to the change in the concentration of the analyte. The position of the corresponding phase change is seen shifting toward the higher incident angle side with the increase of the concentration of SARS-CoV-2 virus, which happens because of the damping of surface plasmons in the structure.

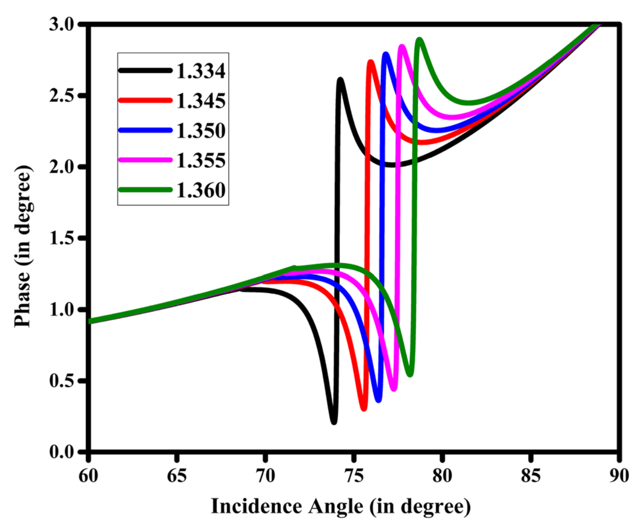


**Fig. 7** Phase shift vs incidence angle plot for final structure

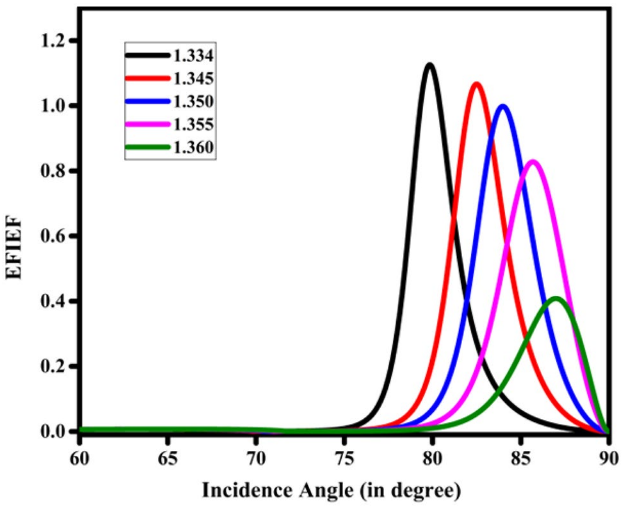


**Fig. 8** EFIEF vs incidence angle plot for final structure

In addition to this, the variation of electric field intensity enhancement factor (EFIEF) with the change in the concentration of SARS-CoV-2 virus, for the final structure, is also analyzed. The EFIEF is a major performance parameter of the SPR-based biosensor and can be mathematically calculated from Eq. (18). The EFIEF defines the effectiveness with which the electric field is confined in SM in contrast to the metal–dielectric interface. At resonance angles for the final structure, the corresponding field peak height is clearly displayed in Fig. 8. Therefore, confirming that most of the incident light energy is transferred to the surface plasmons at resonance angle, resulting in their excitation. Additionally, it is also observed that with the increment in the concentration of the analyte, resulting in the variation of RI from $n_1 = 1.334$ to $n_5 = 1.360$, there is a decrease in EFIEF. This mainly occurs due to the increasingly strong absorption of the incident light energy by the analyte.

## Conclusion

In the present work, for the selective early-stage diagnosis of SARS-CoV-2 virus, a comprehensive investigation of a highly sensitive SPR-based biosensor has been conducted. The biosensor employs a low-RI, $CaF_2$ prism, a SPR-active metal Ag, $TiO_2$, and MXene. Initially, optimization of the thickness of Ag layer was conducted to obtain minimum reflectivity at resonance condition. After tuning the thickness of $TiO_2$ layer and number of MXene layers, maximum angular sensitivity was obtained. The structure-I and structure-II show a sensitivity of 320°/RIU and 178°/RIU but the hybrid structure-III shows a maximum sensitivity of 346°/RIU. The reason is that more SPs are generated because of the high light-trapping ability of $TiO_2$ which eventually increases the resonance angle. For analyzing the performance parameters, a minimum $\Delta n_s = 0.005$ has been taken, confirmed by the TMM technique. As a result, it is concluded that this work may facilitate a significant sensing device for accuracy along with the fast early-stage diagnosis of SARS-CoV-2 virus and may be implemented to identify COVID-19 patients on time.

**Acknowledgements** One of the authors (Swati Srivastava) expresses her gratitude to Madan Mohan Malaviya University of Technology, Gorakhpur, and especially to the Physics and Material Science Department for providing the opportunity and support to carry out this research work.

**Author Contribution** Swati Srivastava: developed a concept, collected data, analyzed, and interpreted it, created a model and methodology, and wrote the first draft. Sachin Singh and Adarsh Chandra Mishra: data gathering, data analysis, interpretation, manuscript review, editing, and creation of the final draft. Pooja Lohia and D. K. Dwivedi: drafted the final version, edited and reviewed the manuscript, and acted as a mentor for the planning and execution of the research activity.

**Data Availability** The dataset generated during analysis is available in the present article.

## Declarations

**Ethics Approval** This is a theoretical study that does not require ethical approval.

**Conflict of Interest** The authors declare no competing interests.

## References

1. Chan KR, Wang X, Saron WAA, Gan ES, Tan HC, Mok DZL, Zhang SLX, Lee YH, Liang C, Wijaya L, Ghosh S, Cheung YB, Tannenbaum SR, Abraham SN, St John AL, Low JGH, Ooi EE (2016) Cross-reactive antibodies enhance live attenuated virus infection for increased immunogenicity. Nat Microbiol. https://doi.org/10.1038/nmicrobiol.2016.164
2. Sankaran N, Weiss RA (2021) Viruses: impact on science and society. In: Encyclopedia of Virology, Elsevier, pp 671–680. https://doi.org/10.1016/b978-0-12-814515-9.00075-8
3. Zhou P, Yang XL, Wang XG, Hu B, Zhang L, Zhang W, Si HR, Zhu Y, Li B, Huang CL, Chen HD, Chen J, Luo Y, Guo H, Di Jiang R, Liu MQ, Chen Y, Shen XR, Wang X, Zheng XS, Chen QJ, Deng F, Liu LL, Yan B, Zhan FX, Wang YY, Xiao GF, Shi ZL (2020) A pneumonia outbreak associated with a new coronavirus of probable bat origin. Nature 579:270–273. https://doi.org/10.1038/s41586-020-2012-7
4. Astuti I, Ysrafil (2020) Severe acute respiratory syndrome coronavirus 2 (SARS-CoV-2): an overview of viral structure and host response, diabetes and metabolic syndrome: clinical research and reviews. Diabetes Metab Syndr Clin Res Rev 14:407–412. https://doi.org/10.1016/j.dsx.2020.04.020
5. Wong SK, Li W, Moore MJ, Choe H, Farzan M (2004) A 193-amino acid fragment of the SARS coronavirus S protein efficiently binds angiotensin-converting enzyme 2. J Biol Chem 279:3197–3201. https://doi.org/10.1074/jbc.C300520200

6. Walls AC, Park YJ, Tortorici MA, Wall A, McGuire AT, Veesler D (2020) Structure, function, and antigenicity of the SARS-CoV-2 spike glycoprotein. Cell 181:281-292.e6. https://doi.org/10.1016/j.cell.2020.02.058
7. Chu DKW, Pan Y, Cheng SMS, Hui KPY, Krishnan P, Liu Y, Ng DYM, Wan CKC, Yang P, Wang Q, Peiris M, Poon LLM (2020) Molecular diagnosis of a novel coronavirus (2019-nCoV) causing an outbreak of pneumonia. Clin Chem 66:549–555. https://doi.org/10.1093/clinchem/hvaa029
8. Singh S, Sharma AK, Lohia P, Dwivedi DK, Singh PK (2020) Design and modelling of high-performance surface plasmon resonance refractive index sensor using $BaTiO_3$, MXene and nickel hybrid nanostructure. Plasmonics 1–14
9. Yuan X, Yang C, He Q, Chen J, Yu D, Li J, Zhai S, Qin Z, Du K, Chu Z, Qin P (2020) Current and perspective diagnostic techniques for COVID-19. ACS Infect Dis 6:1998–2016. https://doi.org/10.1021/acsinfecdis.0c00365
10. Shirato K, Semba S, El-Kafrawy SA, Hassan AM, Tolah AM, Takayama I, Kageyama T, Notomi T, Kamitani W, Matsuyama S, Azhar EI (2018) Development of fluorescent reverse transcription loop-mediated isothermal amplification (RT-LAMP) using quenching probes for the detection of the Middle East respiratory syndrome coronavirus. J Virol Methods 258:41–48. https://doi.org/10.1016/j.jviromet.2018.05.006
11. Li M, Cushing SK, Wu N (2015) Plasmon-enhanced optical sensors: a review. Analyst 140:386–406. https://doi.org/10.1039/c4an01079e
12. Sahoo PR, Swain P, Nayak SM, Bag S, Mishra SR (2016) Surface plasmon resonance based biosensor: a new platform for rapid diagnosis of livestock diseases. Vet World 9:1338–1342. https://doi.org/10.14202/vetworld.2016.1338-1342
13. Yoo H, Shin J, Sim J, Cho H, Hong S (2020) Reusable surface plasmon resonance biosensor chip for the detection of H1N1 influenza virus. Biosens Bioelectron. https://doi.org/10.1016/j.bios.2020.112561
14. Prabowo BA, Wang RYL, Secario MK, Ou PT, Alom A, Liu JJ, Liu KC (2017) Rapid detection and quantification of Enterovirus 71 by a portable surface plasmon resonance biosensor. Biosens Bioelectron 92:186–191. https://doi.org/10.1016/j.bios.2017.01.043
15. Karki B, Ramya KC, Sandhya Devi RS, Srivastava V, Pal A (2022) Titanium dioxide, black phosphorus, and bimetallic layer-based surface plasmon biosensor for formalin detection: numerical analysis. Opt Quantum Electron. https://doi.org/10.1007/s11082-022-03875-6
16. Moznuzzaman M, Khan I, Islam MR (2021) Nano-layered surface plasmon resonance-based highly sensitive biosensor for virus detection: a theoretical approach to detect SARS-CoV-2. AIP Adv. https://doi.org/10.1063/5.0046574
17. Singh S, Sharma AK, Lohia P, Dwivedi DK, Fouad H, Akhtar MS (2022) Sensitivity enhancement of SPR biosensor employing heterostructure blue phosphorus/MoS2 and silicon layer. Emerg Mater Res 11(2):239–250
18. Kumar A, Kumar A, Srivastava SK (2022) Silicon nitride-BP-based surface plasmon resonance highly sensitive biosensor for virus SARS-CoV-2 detection. Plasmonics 17:1065–1077. https://doi.org/10.1007/s11468-021-01589-1
19. Funari R, Chu KY, Shen AQ (2020) Detection of antibodies against SARS-CoV-2 spike protein by gold nanospikes in an opto-microfluidic chip. Biosens Bioelectron. https://doi.org/10.1016/j.bios.2020.112578
20. Bernardi M, Ataca C, Palummo M, Grossman JC (2017) Optical and electronic properties of two-dimensional layered materials. Nanophotonics 6:479–493. https://doi.org/10.1515/nanoph-2015-0030
21. Li Y, Li Z, Chi C, Shan H, Zheng L, Fang Z (2017) Plasmonics of 2D nanomaterials: properties and applications. Adv Sci. https://doi.org/10.1002/advs.201600430
22. Cai S, Yang R (2020) Two-dimensional nanomaterials with enzyme-like properties for biomedical applications. Front Chem. https://doi.org/10.3389/fchem.2020.565940
23. Kim H, Wang Z, Alshareef HN (2019) MXetronics: electronic and photonic applications of MXenes. Nano Energy 60:179–197. https://doi.org/10.1016/j.nanoen.2019.03.020
24. Wu Q, Li N, Wang Y, Liu Y, Xu Y, Wei S, Wu J, Jia G, Fang X, Chen F, Cui X (2019) A 2D transition metal carbide MXene-based SPR biosensor for ultrasensitive carcinoembryonic antigen detection. Biosens Bioelectron. https://doi.org/10.1016/j.bios.2019.111697
25. Chen R, Kan L, Duan F, He L, Wang M, Cui J, Zhang Z, Zhang Z (n.d.) Surface plasmon resonance aptasensor based on niobium carbide MXene quantum dots for nucleocapsid of SARS-CoV-2 detection. https://doi.org/10.1007/s00604-021-04974-z/Published
26. Kumar A, Verma P, Jindal P (2023) Surface plasmon resonance sensor based on MXene coated PCF for detecting the cancer cells with machine learning approach. Microelectron Eng. https://doi.org/10.1016/j.mee.2022.111897
27. Hasib MHH, Nur JN, Rizal C, Shushama KN (2019) Improved transition metal dichalcogenides-based surface plasmon resonance biosensors. Condens Matter 4:1–11. https://doi.org/10.3390/condmat4020049
28. Mostufa S, Akib TBA, Rana MM, Islam MR (2022) Highly sensitive TiO2/Au/graphene layer-based surface plasmon resonance biosensor for cancer detection. Biosensors (Basel). https://doi.org/10.3390/bios12080603
29. Shalabney A, Abdulhalim I (2010) Electromagnetic fields distribution in multilayer thin film structures and the origin of sensitivity enhancement in surface plasmon resonance sensors. Sens Actuators A Phys 159:24–32. https://doi.org/10.1016/j.sna.2010.02.005
30. Shivangani MF, Alotaibi Y, Al-Hadeethi P, Lohia S, Singh DK, Dwivedi A, Umar HM, Alzayed H, Algadi S (2022) Baskoutas, Numerical study to enhance the sensitivity of a surface plasmon resonance sensor with BlueP/WS2-covered Al2 O3-nickel nanofilms. Nanomaterials. https://doi.org/10.3390/nano12132205
31. Pandey AK, Sharma AK (2018) Simulation and analysis of plasmonic sensor in NIR with fluoride glass and graphene layer. Photonics Nanostruct 28:94–99. https://doi.org/10.1016/j.photonics.2017.12.003
32. Singh S, Singh PK, Umar A, Lohia P, Albargi H, Castañeda L, Dwivedi DK (2020) 2D nanomaterial-based surface plasmon resonance sensors for biosensing applications. Micromachines (Basel). https://doi.org/10.3390/mi11080779
33. Singh Y, Raghuwanshi SK (2021) Titanium dioxide (TiO2) coated optical fiber-based SPR sensor in near-infrared region with bimetallic structure for enhanced sensitivity. Optik (Stuttg). https://doi.org/10.1016/j.ijleo.2020.165842
34. Wu L, You Q, Shan Y, Gan S, Zhao Y, Dai X, Xiang Y (2018) Few-layer Ti3C2Tx MXene: a promising surface plasmon resonance biosensing material to enhance the sensitivity. Sens Actuators B Chem 277:210–215. https://doi.org/10.1016/j.snb.2018.08.154
35. Azzam RMA, Bashara NM (1977) Ellipsometry and polarized light, North-Holland Pub. Co
36. Schreiber B, Wacinski C, Chiarello R (2013) Index of refraction as a quality control metric for liquids in pharmaceutical manufacturing. Pharm Eng 33(2):1–7. www.PharmaceuticalEngineering.org
37. Pal S, Prajapati YK, Saini JP (2020) Influence of graphene's chemical potential on SPR biosensor using ZnO for DNA hybridization. Opt Rev 27:57–64. https://doi.org/10.1007/s10043-019-00564-w
38. Balaji VR (2021) Theoretical analysis of tuning and sensitivity improvement of surface plasmon resonance biosensor employing heterostructures of titanium disilicide and graphene. https://doi.org/10.21203/rs.3.rs-705251/v1

39. Verma A, Prakash A, Tripathi R (2015) Sensitivity enhancement of surface plasmon resonance biosensor using graphene and air gap. Opt Commun 357:106–112. https://doi.org/10.1016/j.optcom.2015.08.076
40. Maurya JB, Prajapati YK (2016) A comparative study of different metal and prism in the surface plasmon resonance biosensor having MoS2-graphene. Opt Quantum Electron. https://doi.org/10.1007/s11082-016-0562-6